Estimations of Precipitable Water and Its Characteristics during the HUBEX/IOP 1998

YAO Zhanyu *[1,2](姚展予), XU Chenhai [1](许晨海), YUAN Jian [2](袁 健),
LI Wanbiao [2](李万彪), ZHU Yuanjing [2](朱元竞), and ZHAO Bolin [2](赵柏林)

[1] *Chinese Academy of Meteorological Sciences, Beijing* 100081

[2] *Department of Atmospheric Sciences, School of Physics, Peking University, Beijing* 100871

(Received January 18, 2002; revised November 1, 2002)

ABSTRACT

GMS-5 satellite data at channels of infrared split windows and water vapor are analyzed to retrieve the precipitable water (PW) distributions under cloud-free conditions. Radiosonde data and surface station data are applied to estimate the PW distributions under cloudy conditions. These two methods are then merged to obtain the PW distributions under all-weather conditions during the Huaihe River Basin Energy and Water Cycle Experiment (HUBEX). The results of the all-weather PW distributions from these methods demonstrate that this new merging technique may be applied to derive large-scale or global maps of PW. It is revealed that the atmospheric water vapor over the Yangtze-Huaihe River Basins came mainly from the southwest during the 1998 prevailing period of Meiyu. Sufficient atmospheric PW is a necessary condition for ground rainfall. Under certain dynamic conditions, it can be partially transformed into surface precipitation. Several types of rain are displayed and their PW conditions and characteristics, as well as atmospheric dynamic conditions, are analyzed. It is demonstrated that surface precipitation centers usually appear not at the high PW centers but on their downwind sides.

Key words: precipitable water, estimation technique, all-weather condition, characteristic analysis

1. Introduction

The Huaihe River Basin Energy and Water Cycle Experiment (HUBEX) in China is an important component of the Global Energy and Water Cycle Experiment (GEWEX) and the GEWEX Asian Monsoon Experiment (GAME), in which the study of atmospheric precipitable water (PW) is one of the key items.

Atmospheric PW plays an important role in the energy and water cycle process of the land-atmosphere system. It often directly impacts the evolution of severe weather events. To study the spatial and temporal variations, satellite infrared (IR) remote-sensing data have been used to retrieve PW under cloud-free conditions. Aoki and Inoue (1982) used a single IR channel of the first geostationary meteorological satellite (GMS-1) to estimate PW. Chesters et al. (1983, 1987) and Guillory et al. (1993) retrieved PW from the Visible and Infrared Spin Scan Radiometer (VISSR) Atmospheric Sounder (VAS) split window channels of GOES satellites. Kleespies and McMillin (1990) and Eck and Holben (1994) applied the Advanced Very High Resolution Radiometer (AVHRR) split window channels of NOAA satellites for PW estimation. Zhu et al. (1998) took PW retrieval from the split window channels of the GMS-5 satellite. In this study, we estimate the distribution of PW in the cloud-free atmosphere using data from both the split window channels and the water vapor channel of the GMS-5 satellite.

Previous studies have shown that atmospheric PW is strongly correlated with certain surface meteorological variables, such as water-vapor pressure (Cole, 1976; Yang and Qiu, 1996) and dew point temperature (Smith, 1966; Atwater and Ball, 1976). After analyzing station radiosonde data, we found that PW has a good relationship to surface water-vapor pressure and surface relative humidity.

Using a merging technique, we can obtain the PW distribution and variation under all-weather conditions by combining the retrieved PW from GMS-5 satellite data and the estimated PW from ground-based weather observations.

*E-mail: yaozy@cams.cma.gov.cn

It is well known that 1998 was the second year since the 1997 onset of the strongest El Niño event during the past 100 years. Due to the continually higher sea surface temperature (SST) of the equatorial eastern Pacific Ocean and the continually lower SST of the tropical western Pacific Ocean, the main body of the subtropical high over the western Pacific was located abnormally on the southern and eastern side. This led to the major seasonal rainbelt in East Asia being stationary and continually active in the Yangtze River Basin, which resulted in the excessively severe flooding in this region in the summer of 1998. The 1998 HUBEX intensive observation period (IOP) (11 June 23 July) was undertaken just under this synoptic background, so it had particular scientific significance. According to Ding et al. (1999), the prevailing period of Meiyu in the Yangtze-Huaihe River Basins in 1998 was from 28 June to 3 July, when the concentrated heavy rainfall occurred in the Huaihe River Basin. The main processes of the Meiyu precipitation during this period were well observed by the HUBEX observation network, and the distribution and variation of atmospheric PW in the Huaihe River Basin during this period are particularly analyzed in this study.

2. Data and study region

The GMS-5 satellite data, radiosonde data, and surface weather station data from May to August 1998 in the HUBEX area (28°–40°N, 110°–122°E) were analyzed in this study for the estimation of PW distribution and variation for all-weather conditions.

The GMS-5 VISSR has four channels. The sub-satellite resolution of each channel is shown in Table 1. The GMS-5 IR data from the split window channels and the water vapor channel were used to retrieve the PW distribution under cloud-free conditions.

Table 1. Sub-satellite resolution of each channel of GMS-5

Channel	Visible	IR Split Window		Water Vapor
Wavelength (μm)	0.55–0.90	10.5–11.5	11.5–12.5	6.5–7.0
Resolution (km)	1.25	5		5

There are 21 radiosonde stations and more than 300 surface stations in the HUBEX area. Their distribution is displayed in Fig. 1. The routine observation data from these radiosonde and surface stations were used to estimate the PW distribution under all-weather conditions and to analyze the corresponding characteristics of PW distribution and evolution.

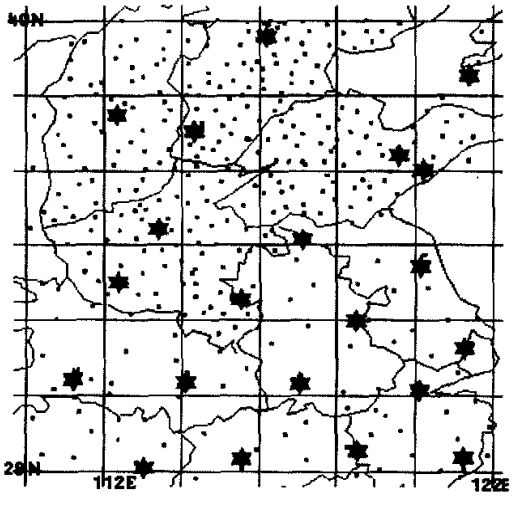

Fig. 1. Distribution of radiosonde stations (stars) and surface stations (points) in the HUBEX area.

3. Estimation of atmospheric PW under all-weather conditions

Satellite remote sensing estimations of PW based upon GMS-5 infrared (IR) data have higher temporal (1-hourly) and spatial (5 km) resolution, but they are only available under cloud-free conditions. On the other hand, the estimation of PW using surface station data can be performed under all-weather conditions, but it has lower temporal (twice or four times a day) and spatial (about 60–70 km) resolution. In order to take advantage of both types of measurement, we employed a merging technique for the combined estimation of PW distribution under all-weather conditions using both the satellite infrared data and surface station data.

3.1 *Retrieval of PW distributions under cloud-free conditions by GMS-5 IR data*

The PW retrieval using satellite IR data is only suitable for cloud-free atmosphere because the IR radiation cannot penetrate cloud layers. The retrieval is based on the infrared radiative transfer equation. Calculated results using a low-resolution transfer model, LOWTRAN7 (Kneizys et al., 1989), have demonstrated that the two IR split window channels and the water vapor channel of the GMS-5 are sensitive to the variations of low-level and upper-level water va-

por contents, respectively. This agrees with the results of Chesters et al. (1983). Therefore a statistical retrieval method using the three channels is offered in this study to estimate atmospheric PW under cloud-free conditions.

Based on the matched radiosonde data and GMS-5 IR data and the method of multivariate linear regression, we obtained the following empirical equation for retrieving PW (mm) under cloud-free conditions over the HUBEX area using the GMS-5 IR data:

$$\mathrm{PW} = -0.045 \times T_1 + 0.190 \times T_{\mathrm{wv}} + 19.859 \times (T_1 - T_2) - 4.427, \quad (1)$$

where the fitted PW was calculated from radiosonde data, T_1 and T_2 are the brightness temperatures at the two split-window channels, respectively, and T_{wv} is the brightness temperature at the water vapor channel. The accuracy statistics for the above empirical expression presented a RMS error of 6.847 mm and a correlation coefficient of 0.792.

3.2 *Estimation of PW distributions under all-weather conditions by radiosonde and surface station data*

PW (mm) can be calculated from radiosonde data as follows:

$$\mathrm{PW} = \frac{1}{g}\int_0^{p_s} q\,(p)\,dp, \quad (2)$$

where g is the gravitational acceleration, q is specific humidity, p is atmospheric pressure, and p_s is surface air pressure.

Analysis of data from the HUBEX region showed that PW has a good relationship with surface water-vapor pressure e (hPa) and surface relative humidity RH (%). These two surface variables account for about 85% of the PW variance. Therefore, we applied the following regression equation to derive PW (mm):

$$\mathrm{PW} = a_1 \cdot e + a_2 \cdot RH + b, \quad (3)$$

where a_1, a_2, and b are regression coefficients. We derived the regression coefficients at each of the 21 radiosonde stations in the HUBEX region. The values vary from 1.471 to 1.994 for a_1, 9.494 to 42.895 for a_2, and −34.057 to −5.480 for b, and the average correlation coefficient of the empirical expressions for the 21 radiosonde stations is 0.817 (Yao et al., 2001).

As shown in Fig. 1, there are much more surface stations with e and RH observations than with radiosonde data. In order to use Eq. (3) at surface stations without radiosonde observations, we need to spatially interpolate the regression coefficients.

Considering the different distances between each radiosonde station and each surface station, the different geographical environment at each radiosonde station and each surface station, and the different relationship between PW and surface atmospheric humidity (e and RH) at each radiosonde station, we define an interpolation weighting function as follows:

$$W_{ij} = \frac{r_j\left[(\varphi_j - \varphi_i)^2 + (\theta_j - \theta_i)^2\right]}{\sum\limits_k r_k\left[(\varphi_k - \varphi_i)^2 + (\theta_k - \theta_i)^2\right]}. \quad (4)$$

Here φ and θ denote latitude and longitude, respectively, r is the correlation coefficient of PW and surface e and RH at a radiosonde station, j denotes the jth radiosonde station, i denotes the ith surface station, W_{ij} is the interpolation weight from the jth radiosonde station into the ith surface station, and k denotes each of the radiosonde stations within a radius of four latitude/longitude degrees (about 400 km) centered at the ith surface station. Therefore the empirical coefficients at the ith surface station can be calculated as follows:

$$C_i = \sum_j W_{ij} \cdot C_j \qquad (C = a_1, a_2, b). \quad (5)$$

Using Eqs. (4) and (5), we obtained the PW regression coefficients at over 300 surface stations in the HUBEX region (Fig. 1).

Because of the much denser distribution of surface weather stations than of radiosonde stations, the estimations of PW distribution based on the former should be better than those based only on the latter. This has been demonstrated by the actual comparison of the PW distribution under all-weather conditions between the estimations based on the data from the 21 radiosonde stations and the ones based on the data from all the surface stations in the HUBEX area (Yao et al., 2001).

3.3 *Combined estimation of PW distribution under all-weather conditions using data from both satellite observations and ground stations*

As we know, the PW retrieval by GMS-5 satellite infrared data only works under cloud-free conditions. For the cloudy regions, only the routine observation (ground-based) data can be used for PW estimation, although they have much lower temporal and spatial resolutions than the satellite data. Therefore a suitable method is needed for the organic combination of the two kinds of data for all-weather PW estimation. A new merging technique is developed in this study for the combined estimation of PW distributions under all-weather conditions using both the satellite infrared data and surface station data. The technique focuses on the comprehensive application of satellite and routine observation data. The GMS-5 infrared data were

used for the retrieval of PW in the cloud-free areas, whereas the surface station data were applied to estimate PW in the cloudy areas. Around the borders of these two areas, a weighted interpolation was applied, with the satellite contributing 90% and the surface stations contributing 10%. These weights were chosen based on our analyses of hundreds of samples in the HUBEX area. It is found that the merging technique works well for estimating the PW distribution over the HUBEX region in 1998 (Yao et al., 2001).

4. Results and analyses of PW distribution and evolution over the HUBEX area during the 1998 prevailing period of Meiyu

By means of the above merging method, we analyzed the corresponding GMS-5 IR data and surface station data and obtained the PW distribution and evolution over the HUBEX area during the 1998 prevailing period of Meiyu. Twenty-nine images of the PW distribution for this region were made (omitted here), an image every 6 hours from 0000 UTC 27 June to 0000 UTC 4 July, which demonstrate the visual PW variation over the Huaihe River Basin during the Meiyu prevailing period.

Figure 2 gives an example of the PW distribution and evolution over the HUBEX area from 0000 UTC 28 June to 1200 UTC 29 June 1998. The streamline field at 850 hPa was superimposed onto each figure. It clearly shows that the atmospheric water vapor over the Huaihe River Basin originated mainly from the southwest. Combined with the stationary Meiyu front over this region, the continual southwest water vapor transportation into this area caused the concentrated heavy rainfalls over the Huaihe River Basin from 28 June to 3 July.

It is well known that sufficient atmospheric PW is a necessary condition for ground rainfall. Usually sufficient atmospheric PW accompanied by certain dynamic conditions or synoptic situation can bring about surface rain. Based on the analysis of each PW image and real-time surface rain, several characteristics about the relation between the atmospheric PW and the surface precipitation were revealed in the HUBEX area during the 1998 prevailing period of Meiyu.

Figure 3 presents a case of PW distribution at 0000 UTC 29 June 1998 and its effect on the surface rain over the HUBEX area. The high PW was distributed mainly to the south of 34°N in this case while a southwest wind prevailed at the 850 hPa level. Subsequent heavy rainfall appeared on the downwind sides of the PW centers. The 12-hour accumulative rain centers at 1200 UTC 29 June appeared at the northern borders of the large-value PW centers, around 33°N. The superimposed 850 hPa streamline field demonstrates clearly that these rain centers were located on the downwind sides of the PW centers, which was a common phenomenon during the 1998 prevailing period of Meiyu in the HUBEX area.

Another case of PW distribution at 1200 UTC 29 June 1998 is shown in Fig. 4. In this case, the folowing rainfall centers also appeared on the downwind sides of the PW centers, around 32°–33°N. The 12-hour rainfall centers at 0000 UTC 30 June 1998 formed a belt-shape region. It can be clearly seen from the superimposed 850 hPa streamline field that this rainbelt was located at the cyclonic shear line. Cyclonic shear rainfall was one of the main precipitation types in the HUBEX area during the 1998 prevailing period of Meiyu.

Cyclonic rainfall was another main precipitation type during the period. An example of this kind of rain is presented in Fig. 5a. The main PW centers over the HUBEX region at 0000 UTC 30 June 1998 were distributed to the south of 33°N. The accumulation of large amounts of PW over the Yangtze-Huaihe River Basins supplied sufficient water vapor for heavy rainfall in this region. The strong cyclone at the 850 hPa level around 31°–32°N at this time provided the dynamic conditions for the subsequent heavy rainfall over this area. The 700 hPa positive vorticity center at the same time (Fig. 5b) was basically consistent with this strong cyclone center, which further indicates that heavy rainfall would occur around this region. The 12-hour rainfall centers at 1200 UTC 30 June 1998 (Fig. 5a) appeared just near the strong cyclone center, as expected. In this case, the rain centers appeared near the PW centers or on the downwind sides of the PW centers, which was mainly determined by the cyclonic dynamic conditions.

During the concentrated rainfall period from 28 June to 3 July 1998, strong convergence precipitation was also very common. Figure 6a provides an example of this kind of rain and the PW condition. At 0000 UTC 1 July 1998, the atmospheric PW was mainly distributed to the south of 34°N. It can be seen from the superimposed 850 hPa streamline field that there was a strong convergence center around the northern border of the high PW area. This strong convergence center was located just on the downwind side of one of the PW centers, and it generated a severe heavy rainfall over this region. The 12-hour rainfall centers at 1200 UTC 1 July 1998 superimposed on Fig. 6a appeared just around this strong convergence center. The 850 hPa divergence field displayed in Fig. 6b clearly indicates the intensity of the conver-

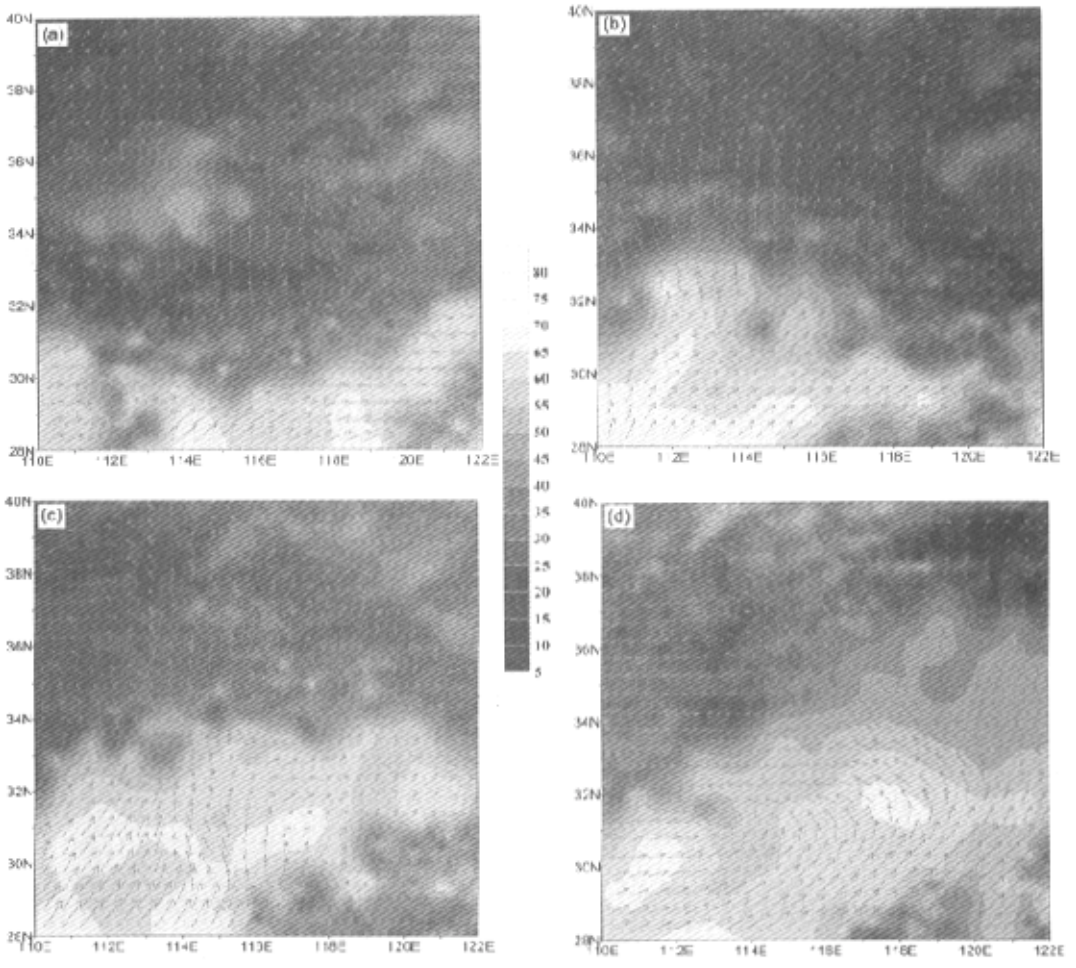

Fig. 2. PW (mm) distribution and evolution superimposed by the 850 hPa streamline field over the HUBEX area at (a) 0000 UTC 28 June, (b) 1200 UTC 28 June, (c) 0000 UTC 29 June, and (d) 1200 UTC 29 June 1998.

gence center. From the 300 hPa divergence field shown in Fig. 6c we can find a corresponding divergence center aloft, located a little east of the low-level convergence center. This was a typical strong convective condition that resulted in the subsequent severe heavy rainfall around the convergence center.

5. Conclusion

By regressing the brightness temperatures from the GMS-5 split-window channels and the water vapor channel against radiosonde-derived PW, an empirical equation for retrieving atmospheric PW under cloud-free conditions over the HUBEX area is obtained. Based on the strong correlation between PW and surface water vapor pressure and relative humidity, empirical equations to estimate PW under all-weather conditions using these parameters are derived from radiosonde and surface data in the HUBEX area. The coefficients in these equations are interpolated with weights to the locations where only the surface observations are available. In order to obtain better results of all-weather PW distributions, the GMS-5 infrared data are used to retrieve the PW of cloud-free areas,

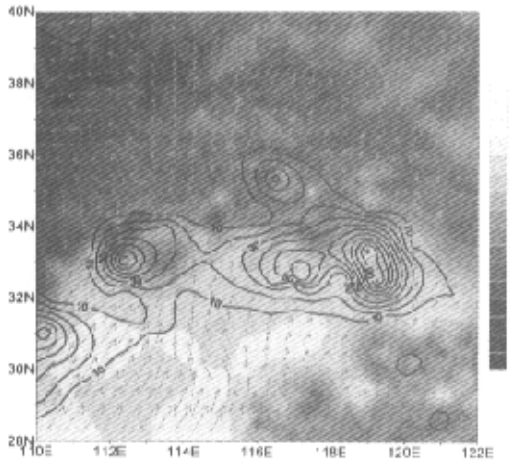

Fig. 3. PW distribution superimposed by the 850 hPa streamline field at 0000 UTC 29 June 1998 and 12 hour rainfall at 1200 UTC 29 June 1998 over the HUBEX area. The filled contour map is the PW (mm) distribution and the black contour lines show the surface rainfall (mm).

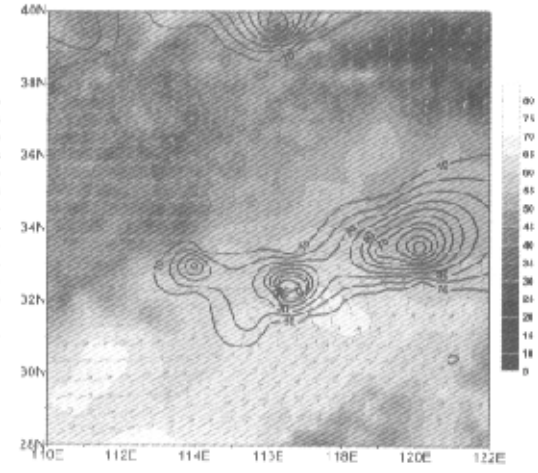

Fig. 4. Same as Fig. 3, but for PW distribution and the 850 hPa streamline field at 1200 UTC 29 June 1998 and 12-hour rainfall at 0000 UTC 30 June 1998 over the HUBEX area.

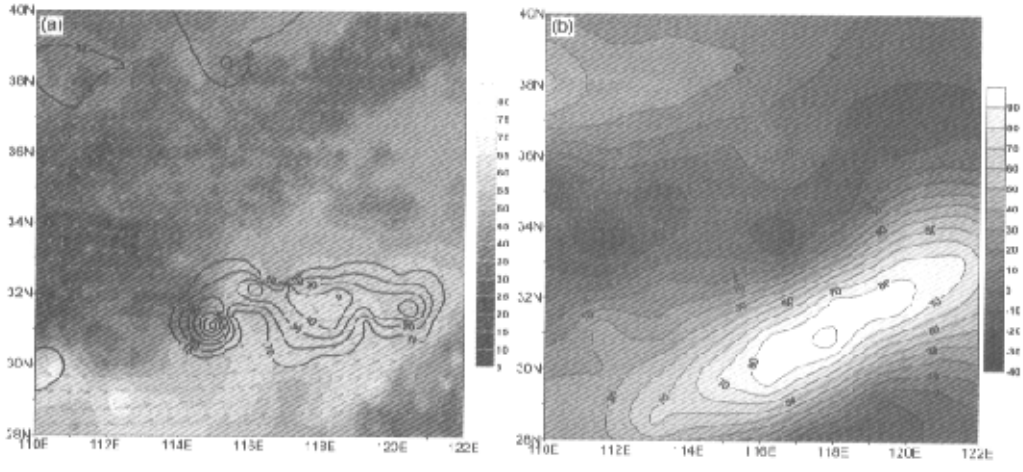

Fig. 5. (a) Same as Fig. 3, but for PW distribution and the 850 hPa streamline field at 0000 UTC 30 June 1998 and 12-hour rainfall at 1200 UTC 30 June 1998 over the HUBEX area, (b) 700 hPa vorticity field (10^{-6} s^{-1}) at 0000 UTC 30 June 1998.

whereas the PW of cloudy regions is derived using the empirical equations and surface data. Around the borders of these two areas, a weighted average of the satellite- and surface-based PW is applied. Using this merging technique, the PW distributions under all-weather conditions are derived for the HUBEX region in central eastern China. Comparisons with cloud maps suggest that the PW distributions derived from

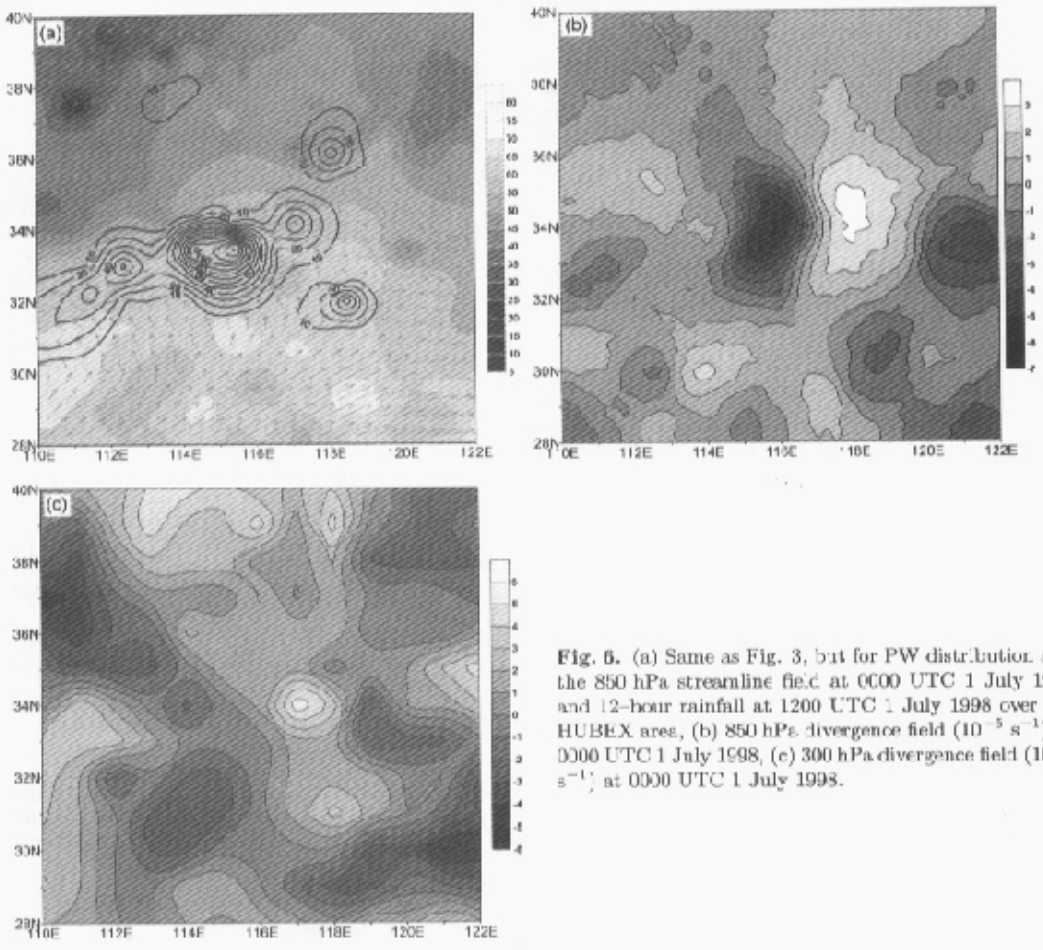

Fig. 5. (a) Same as Fig. 3, but for PW distribution and the 850 hPa streamline field at 0000 UTC 1 July 1998 and 12-hour rainfall at 1200 UTC 1 July 1998 over the HUBEX area, (b) 850 hPa divergence field (10^{-5} s^{-1}) at 0000 UTC 1 July 1998, (c) 300 hPa divergence field (10^{-5} s^{-1}) at 0000 UTC 1 July 1998.

the merging technique reveal finer spatial structures that appear to be realistic. Therefore, this new technique, which takes advantage of both satellite and ground observations, may be applied to derive large-scale and global maps of PW using satellite IR and surface meteorological data.

Twenty-nine PW distribution images, an image every 6 hours from 0000 UTC 27 June to 0000 UTC 4 July 1998, are obtained under all-weather conditions over the HUBEX area based on the proposed technique above. These images visualize the distribution and evolution of atmospheric PW over the HUBEX region during the Meiyu prevailing period of 1998.

It is clearly demonstrated that the atmospheric water vapor over the Yangtze-Huaihe River Basins came mainly from the southwest during the 1998 prevailing period of Meiyu. The continual southwest water vapor transportation formed an accumulation of PW at the stationary Meiyu front over the HUBEX region, which resulted in the concentrated heavy rainfall over this region from 28 June to 3 July 1998.

Sufficient atmospheric PW is not a sufficient condition but merely a necessary condition for ground rainfall. Analyses were conducted to find the dynamic conditions or synoptic situation which play important roles in transforming the atmospheric PW partially into surface precipitation during the HUBEX observational period. It is found that surface precipitation centers usually appeared not at the high PW centers but on their downwind sides. Cyclonic shear rainfall,

cyclonic rainfall, and convergence rainfall were the three main rain types over the HUBEX area during the 1998 prevailing period of Meiyu. The dynamic conditions such as cyclone or convergence as well as sufficient PW in the atmosphere caused this region to experience concentrated heavy rainfall. The cyclonic shear rainfall events usually took place around the cyclonic shear line, which was located on the downwind sides of the high PW centers, and the cyclonic rainfall events often happened near the cyclone centers but not exactly at the center points, which were consistent with the PW centers or on the downwind sides of the PW centers. The convergence rainfall events frequently appeared at the convergence centers situated on the downwind sides of the PW centers.

Acknowledgments. This work was supported by the National Natural Science Foundation of China under the Grant No. 49794030, the National Key Program of Science and Technology of China (2001BA610A-06-05), and the Science Foundation of the China Meteorological Administration and Jilin Provincial Government Joint Laboratory for Weather Modification.

The authors would like to thank Dr. Aiguo Dai, Prof. Fukang Zhu, and the two anonymous reviewers for their efforts in improving the presentation of this paper.

REFERENCES

Aoki, T., and T. Inoue, 1982: Estimation of precipitable water from the IR channel of the geostationary satellite. *Remote Sens. Environ.*, **12**, 219–228.

Atwater, M. A., and J. T. Ball, 1976: Comparisons of radiation computations using observed and estimated precipitable water. *J. Appl. Meteor.*, **15**, 1319–1320.

Chesters, D., L. W. Uccellini, and W. D. Robinson, 1983: Low-level water vapor fields from the VISSR atmospheric sounder (VAS) "split window" channels. *J. Climate Appl. Meteor.*, **22**, 725–743.

Chesters, D., W. D. Robinson, and L. W. Uccellini, 1987: Optimized retrievals of precipitable water from the VAS split window. *J Climate Appl. Meteor.*, **26**, 1059–1066.

Cole, R. J., 1976: Direct solar radiation data as input into mathematical models describing the thermal performance of buildings II: Development of relationships. *Build. Environ.*, **11**, 181–186.

Ding, Y., Y. Zhang, Q. Ma, X. Cao, and X. Liu, 1999: Weather situation and the main achievement during intensive observation of Huaihe River Basin Energy and Water Cycle Experiment in the summer of 1998, *Study of Energy and Water Cycle over Huaihe River Basin* (I). China Meteorological Press, Beijing, 1–11. (in Chinese)

Eck, T. F., and B. N. Holben, 1994: AVHRR split window temperature differences and total precipitable water over land surfaces. *Int. J. Remote Sens.*, **15**, 567–582.

Guillory, A. R., G. J. Jedlovec, and H. E. Fuelberg, 1993: A technique for deriving column-integrated water content using VAS split-window data. *J. Appl. Meteor.*, **32**, 1226–1241.

Kleespies, T. J., and L. M. McMillin, 1990: Retrieval of precipitable water from observations in the split window over varying surface temperature. *J. Appl. Meteor.*, **29**, 851–862.

Kneizys, F. X., E. P. Shettle, L. W. Abreu, G. P. Anderson, J. H. Chetwynd, W. O. Gallery, J. E. A. Selby, and S. A. Clough, 1989: Atmospheric transmittance/radiance: The LOWTRAN 7 model, AFGL-TR-89-XXXX.

Smith, W., 1966: Note on the relationship between total precipitable water and surface dew point. *J. Appl. Meteor.*, **5**, 726–727.

Yang, J., and Qiu J., 1996: The empirical expressions of the relation between precipitable water and ground water vapor pressure for some areas in China. *Scientia Atmospherica Sinica*, **20**(5), 620–626. (in Chinese)

Yao, Z., Yuan J. , Li W., Zhu Y., and Zhao B., 2001: Estimation of water vapor distribution using combined data from GMS-5 and ground stations. *Climate Environ. Res.*, **6**, 197–202. (in Chinese)

Zhu, Y., Li W., and Chen Y., 1998: Study of total precipitable water by GMS-5. *Quart. J. Appl. Meteor.*, **9**, 8–14. (in Chinese)

1998年淮河试验加密观测期间大气可降水的估算及其特征分析

姚展予 许晨海 袁 健 李万彪 朱元竞 赵柏林

摘 要

利用GMS-5卫星红外分裂窗通道和水汽通道资料反演晴空大气的可降水分布，同时利用探空站资料和地面站资料估算云天大气的可降水分布。将这两种方法进行融合，得到淮河流域能量与水分循环试验期间全天候的大气可降水分布。结果表明，这种新的融合技术可应用于确定大尺度或全球尺度的大气可降水分布图像。揭示了江淮流域1998年梅雨盛行期大气中的水汽主要来源于西南方向。充足的大气可降水是产生地面降水的必要条件，在某些动力条件的影响下，空中的大气可降水将部分地被转化为地面降水。给出了几种主要的降水类型，分析了相应的大气可降水条件及其特征，并剖析了产生降水的大气动力条件。结果显示，地面降水中心通常并非出现在大气可降水的高值中心区域而是产生在其下风方向的某一区域。

关键词：大气可降水，估算技术，全天候条件，特征分析